chemosensors

MDPI

Article

Electrodeposition of Au Nanoparticles on 2D Layered Materials and Their Applications in Electrocatalysis of Nitrite

Oana Elena Carp [1], Mirela-Fernanda Zaltariov [2], Mariana Pinteala [1] and Adina Arvinte [1,*]

[1] "Petru Poni" Institute of Macromolecular Chemistry, Centre of Advanced Research in Bionanoconjugates and Biopolymers, Grigore Ghica Voda Alley 41A, 700487 Iasi, Romania; rachita.oana@icmpp.ro (O.E.C.); pinteala@icmpp.ro (M.P.)

[2] "Petru Poni" Institute of Macromolecular Chemistry, Department of Inorganic Polymers, Grigore Ghica Voda Alley 41A, 700487 Iasi, Romania; zaltariov.mirela@icmpp.ro

* Correspondence: adina.arvinte@icmpp.ro; Tel.: +40-332-880-050-555

Abstract: This study presents a comparative analysis of gold nanoparticles electrodeposited on different two-dimensional materials used as electrode substrates, graphene (Gr) and MoS_2, or co-deposited with the metallic material MoS_2. The morphological and electrochemical data demonstrate the efficiency of the electrodeposition process and the preferability of gold nanoparticles for certain attachment sites depending on the nature of the material used as a substrate and the deposition method used. The electrocatalytic activity of the gold nanoparticles obtained in these configurations was evaluated via the oxidation of nitrite ions (NO_2^-), using both qualitative and quantitative approaches, by cyclic voltammetry and amperometry techniques. The electrocatalytic activity of gold nanoparticles co-deposited with MoS_2 is superior compared to that of gold nanoparticles deposited either on bare gold electrodes or on 2D materials (graphene and MoS_2), showing good performance with a specific sensitivity of 1.043 μA μM^{-1} cm^{-2} on the linear range of 0.5–600 μM nitrite, with a limit of detection of 0.16 μM and good anti-interference ability.

Keywords: electrodeposition; 2D materials; nitrite oxidation

check for updates

Received: 1 April 2025
Revised: 30 April 2025
Accepted: 6 May 2025
Published: 12 May 2025

Citation: Carp, O.E.; Zaltariov, M.-F.; Pinteala, M.; Arvinte, A. Electrodeposition of Au Nanoparticles on 2D Layered Materials and Their Applications in Electrocatalysis of Nitrite. *Chemosensors* **2025**, *13*, 180. https://doi.org/10.3390/chemosensors13050180

Copyright: © 2025 by the authors. Licensee MDPI, Basel, Switzerland. This article is an open access article distributed under the terms and conditions of the Creative Commons Attribution (CC BY) license (https://creativecommons.org/licenses/by/4.0/).

1. Introduction

Two-dimensional materials (2DMs) are generally ultrathin layered structures, one to a few atom- or monomer-unit, atomically ordered in networks with strong in-plane bonds and weak van der Waals bonds between layers. Due to the unique physical and chemical properties, such as large surface areas, morphology tunability, excellent mobility, and the possibility to change their surface properties, 2DMs are considered to have great potential for applications in various fields such as optics, energy, electronics, biotechnology, sensors and biosensors [1–6].

Graphene, the first discovered 2D material, is a carbon-based nanomaterial developed in 2004 that takes the shape of a sp2 carbon sheet with atoms bonded together in a honeycomb lattice structure [7,8]. Its superior qualities, such as high intrinsic mobility, exceptional malleability and impermeability, a large theoretical specific surface area (2630 m^2/g for a single layer), and excellent electron transport capabilities, make it a promising material for a wide range of applications, particularly in electronic devices [8–10]. Aside from graphene, several 2D materials have received a lot of attention due to their diverse and distinctive physical and chemical properties [11]. Up to the present, aside from carbon-based 2D materials, transition metal dichalcogenides (molybdenum disulfide, niobium disulfide, titanium diselenide) have also risen to the forefront of research because of their

structural resemblance to graphene [7,12]. Among them, 2D layered molybdenum disulfide (MoS_2), consisting of an Mo atomic layer sandwiched between two S atomic layers held together by weak out-of-plane van der Waals bonds [13], has emerged as one of the most promising sensing materials for building high-performance electrochemical sensors and biosensors [14,15]. MoS_2 is often used as a substitute for graphene. It offers a wide range of potential practical uses in nano-electronics, energy storage, photocatalysts, optical sensors, and electrochemical biosensors.

The attractiveness of this kind of materials primarily lies in their layer or sheet numbers, which significantly impact various properties, particularly electrical characteristics. Additionally, their substantial surface area-to-thickness ratio results in exceptionally high surface areas. At present, there are numerous publications concerning both graphene [16–19], and MoS_2 [20–22] as the most popular 2D materials, widely studied either by themselves or in the form of composites made by merging them with other electroactive materials such as nanoparticles [23–25] and polymers [26], seeking to enhance their electrochemical properties. However, MoS_2, as a transition metal disulfide, is a semiconductor with poor conductivity, and metal nanoparticles are often introduced to improve the conductivity of MoS_2 in different applications [27–29].

Noble metal nanoparticles have become favorite materials in electroanalysis due to their small dimensions and catalytic activities. Gold nanoparticles (AuNPs) are particularly promising for the development of electrochemical sensors owing to their excellent conductivity, high surface area, and strong affinity for specific chemical species. However, the aggregation and instability of AuNPs may pose challenges when using them in electrochemical sensing. To address these drawbacks, one approach is to anchor AuNPs onto different supporting materials. Both graphene and MoS_2 have emerged as ideal supports for AuNPs due to their unique properties, including high surface areas and abundant surface functional groups [30,31].

Graphene sheets decorated with gold nanoparticles have found applications in a wide range of fields, many of these applications depending on the size and morphology of the Au deposits, which are dictated by the deposition method. The integration of Au nanoparticles with graphene has been applied to non-enzymatic glucose sensing [32], detecting hydrogen peroxide [33], ascorbic acid [34], melamine [35], and mercury [36,37], and also for nitrite detection in food [38]. Gold nanoparticles exhibit excellent catalytic properties for nitrite oxidation. Consequently, the synergistic effect of gold and graphene materials was studied in many combinations [39–42] for nitrite electrochemical detection. Similarly, nanoflowers composed of MoS_2 nanosheets and modified by Au nanoparticles to make Au@MoS_2 nanocomposites were prepared and successfully proposed as biosensors for the detection of nitrite [43,44].

Nitrite (NO_2^-) is an inorganic compound widely found as pollutant in the environment, in fertilizers and pesticides, in the food industry as a preservative and food additive and in the chemical industry. While the instant consumption of nitrite may not present immediate health hazards, long-term exposure to food or water with elevated nitrite levels carries potential risks. Nitrite ions within the human body can react with hemoglobin, leading to the formation of methemoglobin, a harmful substance that disrupts oxygen transport, resulting in a condition referred to as "blue baby syndrome". In this context, there is a growing interest for simple and sensitive instruments for the quantitative analysis of nitrites, and AuNPs have been widely introduced in the electrochemical sensing interface to enhance the analytical performance of nitrite [45–49].

Using a variety of electrodeposition procedures and different experimental settings, different AuNP morphologies can be obtained on an electrode's surface [50–52]. Single-step electroreduction has exhibited attractive applications to attach the gold nanoparticle-to the

electrode materials—the size and shape of the electrode can be easily tuned by altering experimental parameters and no stabilizer/capping agents are required.

In this study, we conduct a comparative analysis of the electrodeposition of gold nanoparticles, employing the two-dimensional materials graphene and MoS_2 as electrode substrate materials and assessing their performance as detectors of nitrite ions (NO_2^-). The electrocatalytic impact of these electrode configurations on the oxidation of NO_2^- anions is systematically assessed through both qualitative and quantitative approaches, utilizing cyclic voltammetry and chronoamperometry techniques. Our findings reveal many similarities between gold deposition on graphene and MoS_2 when used as substrates for nitrite electrochemical detection. The difference is in the case of co-deposition of gold with MoS_2, which leads to improved efficiency of deposition and, consequently, enhanced nitrite detection.

2. Materials and Methods

2.1. Reagents

Molybdenum disulfide (MoS_2 98%, powder < 2 μm), gold(III) chloride ($HAuCl_4$ > 99.9%), sulfuric acid (H_2SO_4 98.08 g/mol), sodium nitrite ($NaNO_2 \geq 99.0\%$), sodium nitrate ($NaNO_3 \geq 99.0\%$), magnesium chloride ($MgCl_2 \geq 98.0\%$), sodium chloride ($NaCl \geq 99.0\%$), calcium chloride ($CaCl_2 \geq 99.9\%$), sodium carbonate ($NaCO_3$ > 99.0%), potassium chloride ($KCl \geq 99.0\%$), ammonium carbonate $(NH_4)_2CO_3$ > 99.9%), ascorbic acid ($C_6H_8O_6 \geq 99.0\%$) and glucose ($C_6H_{12}O_6 \geq 99.0\%$) were purchased from Sigma-Aldrich (www.sigmaaldrich.com). Graphene nanopowder (8 mm flakes) was purchased from Graphene Laboratories Inc., Ronkonkoma, NY, USA (https://graphene-supermarket.com). All of the chemical reagents used were analytical grade and did not require further purification. Throughout the experiment, we used ultrapure water to prepare all solutions.

2.2. Apparatus and Methods

The electrochemical measurements were conducted using an AutoLab PGSTAT 302N (Eco Chemie, Utrecht, The Netherlands) potentiostat. All experiments were carried out in a conventional electrochemical cell (10 mL volume) using H_2SO_4 0.1 M as electrolyte and a three-electrode system with a planar configuration of a screen-printed gold electrode (SPE), manufactured and purchased from Metrohm DropSens (MDS, http://www.dropsens.com/), Llanera, Spain. The reference was a silver electrode, while working (4 mm diameter) and counter electrodes were made of gold. Scanning electron microscopy (SEM) was performed on a Quanta 200-FEI scanning electron microscope (FEI company, Hillsboro, OR, USA). Fourier transform infrared (FTIR) spectra were recorded on a Bruker Vertex 70 FTIR spectrometer (Bruker, Ettlingen, Germany) by using KBr pallets in the transmission mode, in the range 400–4000 cm^{-1} at room temperature with a resolution of 2 cm^{-1}.

The cyclic voltammetry technique (CV) was utilized to preliminarily analyze the nucleation and deposition of Au nanoparticles onto different substrates and to evaluate their redox behavior. Amperometric measurements were involved in testing the obtained gold nanoparticles modified electrodes for nitrite oxidation, applying the proper potential.

2.3. Preparation of the Modified Electrodes

The dispersions of 2 mg/mL MoS_2 and graphene and the solution of $HAuCl_4$ 10 mM used for electrodeposition were prepared in 0.5 M sulfuric acid. Both dispersions of 2D materials were homogenized for one hour in an ultrasound bath at room temperature. Two different working protocols were used to prepare the modified electrodes, as presented in Figure 1.

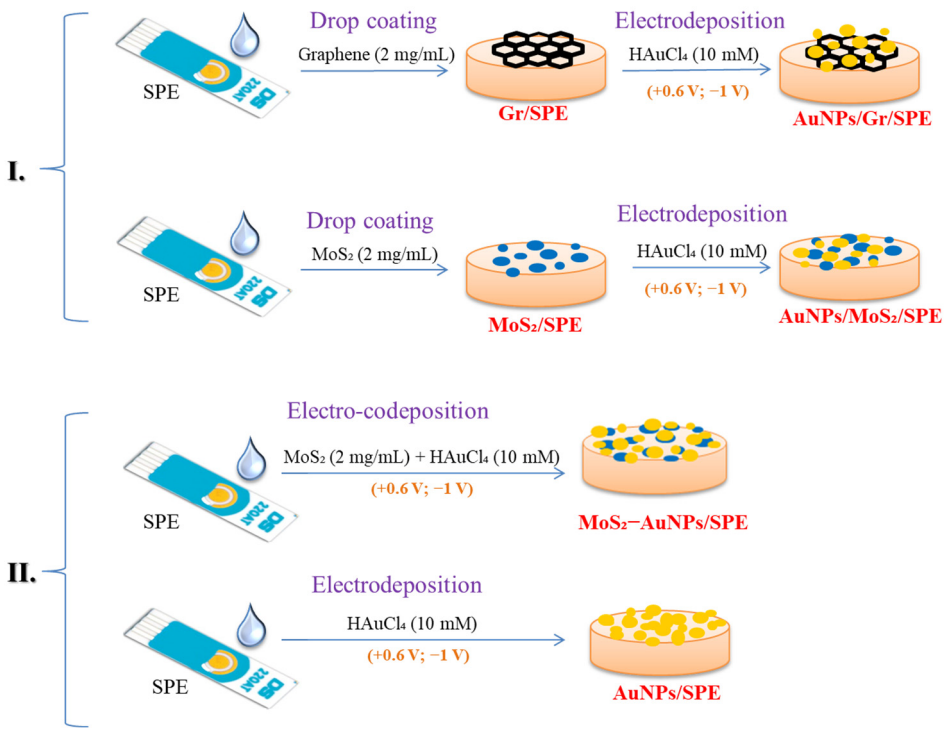

Figure 1. Schematic protocol used for the preparation of gold nanoparticles and 2D materials modified electrodes.

Method I involves two steps. Step 1: Modification of the gold working electrode surface with 2D materials (Gr, MoS_2) by drop coating 2 µL of Gr with 2 mg/mL of MoS_2 and drying for 1 h. Step 2: On the 2D material-modified electrode, gold nanoparticles were electrodeposited from 10 mM of $HAuCl_4$ solution by cyclic voltammetry, sweeping the potential in the +0.6 V and −1 V range for 3 cycles with a scan rate of 0.1 V/s. Small volumes of 100 µL of $HAuCl_4$ 10 mM were used for electrodeposition, placing the drop on the planar surface of the screen-printed electrode (SPE) system so as to cover the three electrodes. Using this protocol, two configurations were made for the modified electrodes, denoted as AuNPs/Gr/SPE and AuNPs/MoS_2/SPE.

Method II—involves the co-deposition of MoS_2 and Au nanoparticles directly on the bare electrode; the nanoparticles are taken from a 100 µL mixture consisting of MoS_2 2 mg/mL and $HAuCl_4$ 10 mM and placed on the surface of the SPE. Then we swept the potential in the range between +0.6 V and −1 V for 3 cycles. The electrode thus obtained is denoted as MoS_2-AuNPs/SPE. Also, for a control comparison, pure AuNPs without any 2D materials were electrodeposited directly on the bare electrode, generating the AuNPs/SPE configuration.

The optimal number of potential scanning cycles for electrodeposition was determined through a systematic investigation of various cycles, allowing for an accurate assessment of the electrodeposition process. Also, the concentration of MoS_2 involved in the co-deposition with gold nanoparticles was carefully chosen after optimization through experimental studies. After the electrodeposition, the electrodes were rinsed with distilled water, dried at room temperature for 1 h, and ready to be used for further assays.

3. Results

3.1. AuNPs Electrodeposition Process

The electrodeposition of AuNPs onto the two 2D materials was performed by cyclic voltammetry using the protocol described in Section 2 (Figure 1). Figure 2 shows the CV

plots of the electrodeposition within the large potential range; the inset zooms in on the cathodic peaks characteristic of the reduction process of gold ions (Au^{3+}) to metallic gold (Au^0) according to the reaction 1 [53,54]. A low negative potential (<−0.4 V) applied in the electrodeposition is essential for a controlled nucleation and growth of the AuNPs [52]. In this study, we applied −1 V as the negative limit of the potential range to ensure the growth rate of the AuNPs, but the effective reduction of ions to metallic gold takes place around 0.4 V. This is the reason we emphasized this region in the inset figure. These cathodic peaks appear at different potential values (0.39; 0.42; 0.45 and 0.47 V), depending on the nature of the material used as the substrate on the electrode or the involved method. With scanning to more negative potentials, a sharp increase in the reduction current at negative potential (around −0.3 V) is attributed to the reduction of water, resulting in the formation of hydrogen gas. On the anodic–going scan, the sharp peak at ca. −0.15 V corresponds to the surface oxidation of the electrodeposited gold [55].

$$AuCl_4^-(aq) + 3e^- \rightarrow Au(s) + 4Cl^- \quad (1)$$

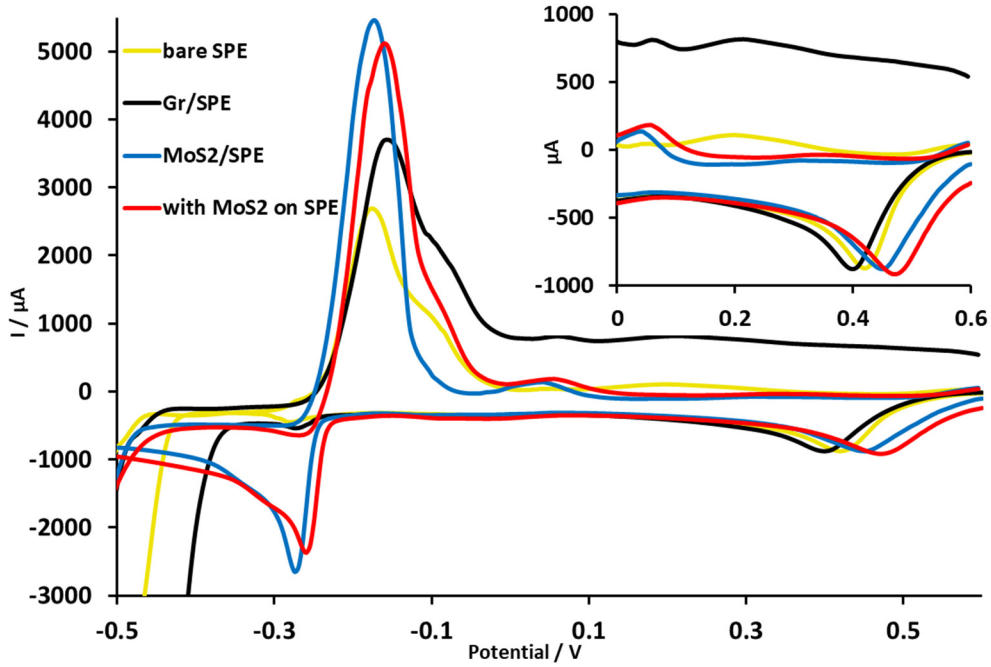

Figure 2. CVs of $HAuCl_4$ 10 mM using different electrode substrates: bare SPE (yellow), Gr/SPE (black), MoS_2/SPE (blue), and for $HAuCl_4$ 10 mM in presence of MoS_2 2 mg/mL (red).

Usually, the electrodeposition of AuNPs is influenced by the nature of the electrode used, specifically by the material deposited as the substrate on the electrode. In this study, Figure 2 shows the reduction peak of Au^{3+} on the Gr-modified electrode at 0.39 V (black line), with a slight shift toward a lower potential compared to the reduction peak that appeared 0.42 V on the bare electrode (yellow line), which we used as a reference. In the case of Au^{3+} reduction on the MoS_2-modified electrode (blue line), a shift toward a higher potential value (0.45 V) (blue line) is observed compared to the reduction peak on the bare electrode. These shifts of the cathodic peak indicate that gold is reduced more easily on the metallic MoS_2 material and less easily on the carbonaceous Gr material compared to the reduction on the bare Au electrode. A possible explanation for this phenomenon is the presence of defects on the surface and edges of the MoS_2 material, areas where sulfur atoms are partially unbound [56,57] and can interact with gold ions forming the

nuclei. These areas act as preferential sites for the formation of metal nuclei, facilitating the cathodic reduction of Au^{3+} to Au^0. The fact that defects and edges on MoS_2 contain partially unbound sulfur, which can act as sites for decoration with noble metal NPs, such as gold, silver, palladium, and platinum was treated by different research groups (T.S. Sreeprasad et al. [56]; J. Zhou et al. [57]) based on the well-established affinity of gold for sulfur [58].

In the case of co-deposition of gold in the presence of MoS_2 (red line) the reduction peak appears at 0.47 V, slightly shifted to a higher potential value compared to the peaks obtained for the other studied configurations. It is known that certain elements, like Mo, W, and Ti, cannot be obtained electrochemically from aqueous solutions [59], but the electrochemical deposition of these metals can be induced by co-deposition with other metals. The induced co-deposition of molybdenum with iron group metals has been extensively investigated [60], showing that depending on concentrations, mass transport of either molybdate or iron group metal species may influence the deposition rate of molybdenum. The divalent iron group species in the electrolyte participate in the reduction of molybdate, involving an adsorbed molybdenum-iron group metal reaction intermediate. The presented model described the catalyzing or "inducing" effect of different iron group elements on the molybdenum reduction.

Fourier Transform Infrared Spectroscopy (FTIR) was used to detect changes in vibrational modes, which can indicate the presence of specific chemical bonds. The FTIR spectra were collected for solutions of MoS_2, $HAuCl_4$ and a mixture of MoS_2 + $HAuCl_4$ (before applying the potential for electrochemical reduction of Au^{3+}). The differences appeared in the IR spectrum of MoS_2 + $HAuCl_4$ and were better highlighted by the "subtract spectra" procedure in OPUS 6.5 software. The resulting subtracted spectrum (Figure 3) revealed maximum (in red color) and minimum (in black color) peaks. The minimum peaks correspond to the common bands found in both the initial MoS_2 and $HAuCl_4$, while the maximum peaks are specific for the MoS_2 + $HAuCl_4$ mixture. MoS_2 shows two distinct bands at 384 and 444 cm^{-1}. After mixing with $HAuCl_4$, the band at 384 cm^{-1} disappeared, while the band at 444 cm^{-1} was blueshifted by 22 cm^{-1}, supporting the interaction between Au and S. The other specific peaks marked in red are characteristic of a sulfuric acid medium.

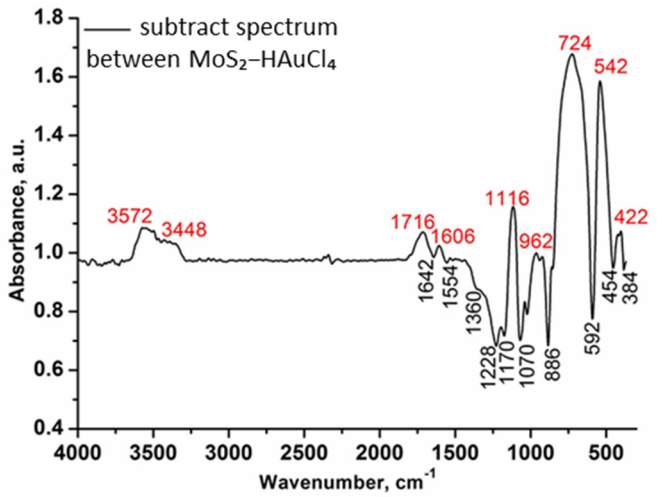

Figure 3. FTIR spectra of solution mixture MoS_2 + $HAuCl_4$.

Experimental evidence from our study suggests that gold ions can interact with and anchor onto the surface of MoS_2 even prior to the application of an external potential. This anchoring behavior is attributed to the strong chemical affinity between gold atoms and the sulfur atoms present in the MoS_2 lattice. Furthermore, as reported in previous

studies [61,62], the presence of dissolved oxygen in the acidic solution promotes the dissociation of Mo–S–Mo bonds, which increases the density of structural defects and edge sites within the MoS_2 material [63]. These defect-rich regions serve as favorable sites for gold nucleation. Consequently, the incorporation of MoS_2 into the acidic electrodeposition solution significantly enhances the interaction between the substrate and Au^{3+} ions, thereby facilitating a more efficient and uniform nucleation process.

3.2. Morphological Characterization of the Modified Electrodes

SEM analysis was conducted to investigate the surface morphology of the prepared chemically modified electrodes labeled as AuNPs/SPE, AuNPs/Gr/SPE, AuNPs/MoS_2/SPE, and MoS_2-AuNPs/SPE. This aimed to discern variations in the deposition of gold particles on each distinct substrate and under different conditions.

Figure 4 compares the SEM image of the pristine bare gold electrode before any modification (Figure 4a) and the image of the electrode with AuNPs electrodeposited directly on it (Figure 4b) according to the protocol described in the experimental method. The bare gold electrode has a reticulated structure, having very large pores with a smooth gold surface. The electrodeposited gold nanoparticles were anchored on this structure, thus increasing the surface roughness and the active surface area of gold that will be involved in electrochemical reactions.

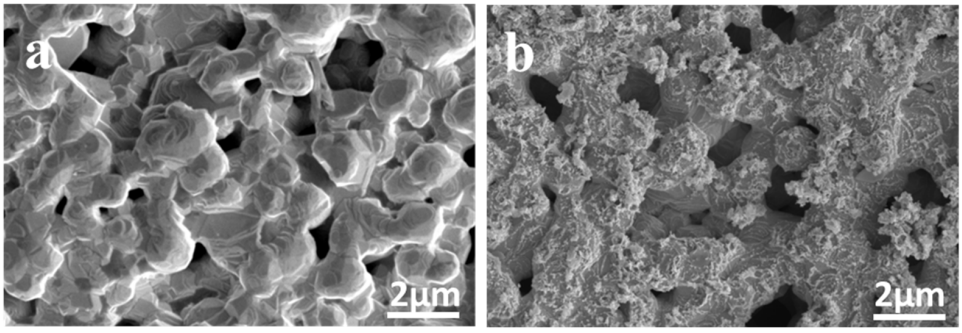

Figure 4. SEM images of (**a**) bare gold SPE and (**b**) AuNPs/SPE electrodes.

In contrast to the porosity depicted on the gold electrode surface in Figures 4 and 5a–c emphasizes the existence of lamellar graphene and MoS_2 structures characterized by diverse sizes ranging from tens of nanometers to several micrometers. These structures are stacked together, creating an expanded surface area with numerous sites favorable for the nucleation and growth of gold nanoparticles, surpassing the potential of the bare electrode. The electrodeposition process results in the uniform growth and distribution of AuNPs on the surface of the Gr substrate, but a limited deposition in the interlamellar spaces. For MoS_2, AuNPs are predominantly situated along the edges of the MoS_2 substrate and at defect sites. These areas, as highlighted in the observations discussed in Section 3.1 on electrodeposition, serve as preferential zones for the formation of metallic nuclei.

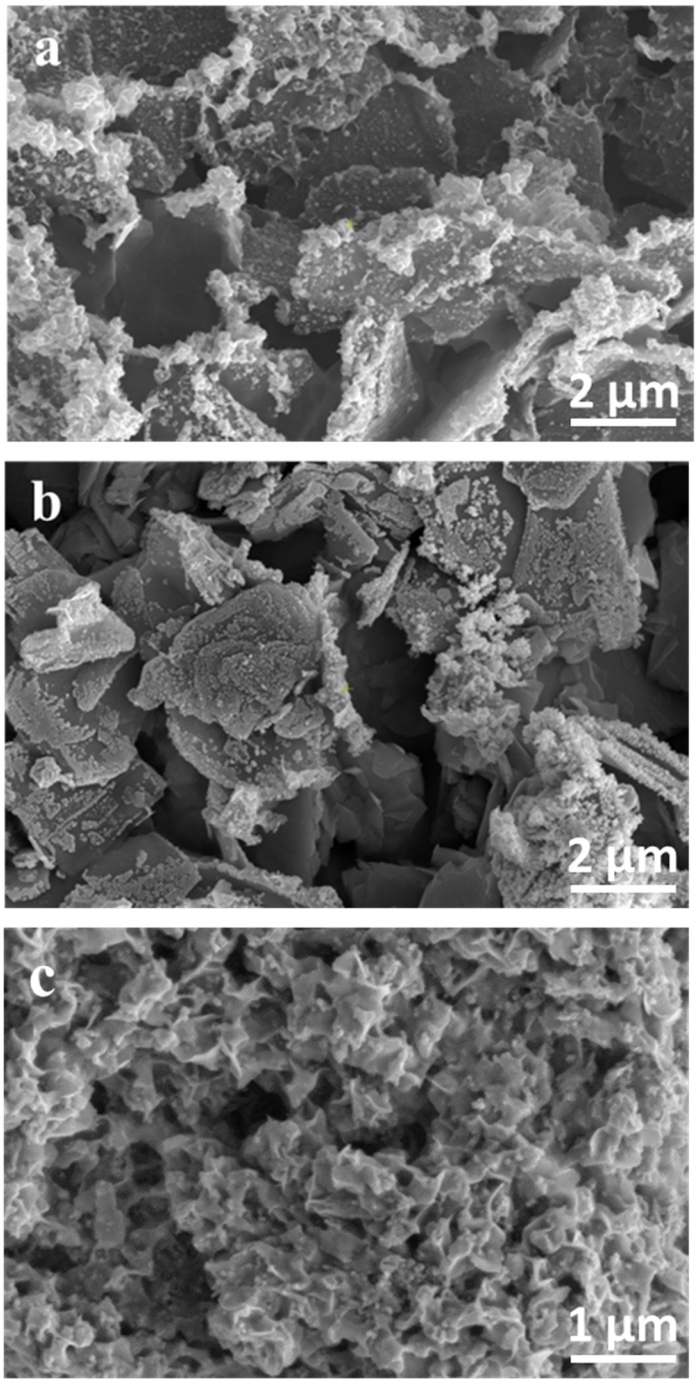

Figure 5. SEM images of: (**a**) AuNPs/Gr/SPE, (**b**) AuNPs/MoS_2/SPE and (**c**) MoS_2-AuNPs/SPE.

Figure 5c shows AuNPs co-deposited with MoS_2 on the surface of the SPE electrode. In this case, the MoS_2 lamellae are no longer discernible, but the formed structure increases the porosity. There is a heightened population density of gold nanoparticles across the entire surface due to an increased number of preferential zones; this aligns with the earlier discussions on co-deposition. SEM analysis highlights the efficiency of the electrodeposition process and the preference of AuNPs for certain attachment sites.

3.3. Electrochemical Characterization of AuNPs Electrodeposited on Different Substrates

The electrochemical activity of AuNPs electrodeposited in three configurations—AuNPs/Gr/SPE, AuNPs/MoS_2/SPE, and MoS_2-AuNPs/SPE—was assessed through cyclic voltammetry in a 0.1 M H_2SO_4 electrolyte. The results were compared with the activity of AuNPs elec-

trodeposited on bare gold electrodes employed as a control experiment (Figure 6). The voltammograms reveal distinctive anodic peaks specific to the gold oxidation process, as defined by the following reactions:

$$Au - (H_2O)ads \rightarrow Au - OH + H^+ + e^- \quad (2)$$

$$Au - OH \rightarrow Au = O + H^+ + e^- \quad (3)$$

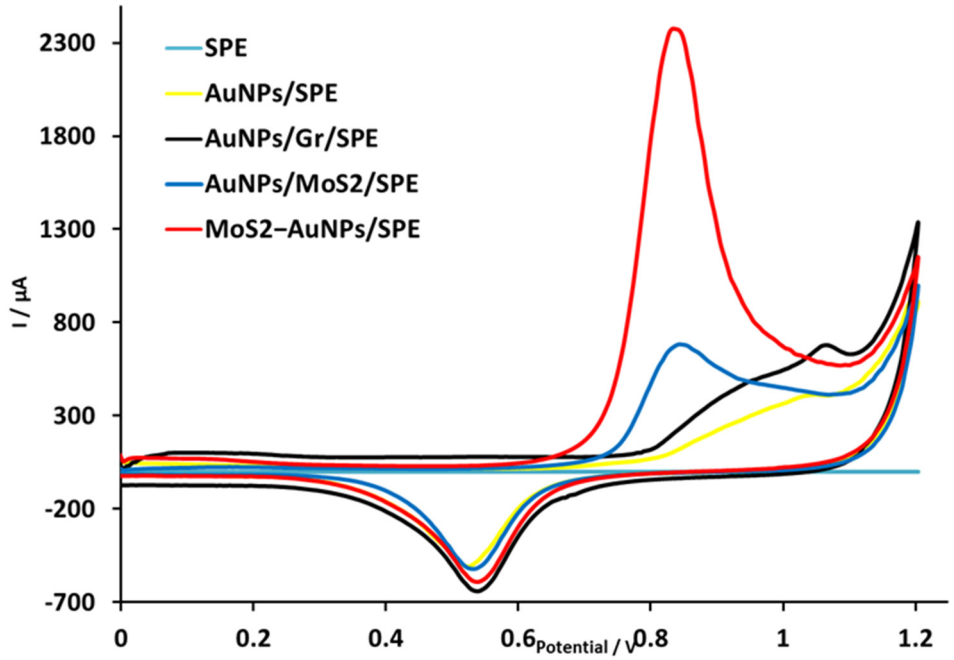

Figure 6. Cyclic voltammograms for AuNPs/SPE (yellow), AuNPs/Gr/SPE (black), AuNPs/MoS_2/SPE (blue) and MoS_2_AuNPs/SPE (red) in 0.1 M H_2SO_4.

The electrooxidation of gold in an acidic medium has been intensively investigated in numerous studies reported in the literature [61–64], which explains the initial formation of an Au-OH monolayer (reaction (2)) on the gold surface in the presence of oxygen species from solution, followed rapidly by oxidation to a mixture of Au(II) and Au(III) oxides (reaction (3)). The size of the peak and its potential are directly determined by the density and number of AuNPs deposited on the electrode surface as well as by their size [65]. The parameters of the obtained anodic peaks are summarized in Table 1 according to the nature of the material used as the substrate on which the gold particles were deposited.

Table 1. Potential and peak height characteristic of AuNPs oxidation deposited in the four configurations.

Modified Electrode	E_{ox} (V)	H_{ox} (mA)
AuNPs/SPE	1.03	0.41
AuNPs/Gr/SPE	1.06	0.56
AuNPs/MoS_2/SPE	0.84	0.62
MoS_2-AuNPs/SPE	0.83	1.9

The differences in the anodic peak height signify an amplified electronic transfer in the case of gold nanoparticles co-deposited with MoS_2, surpassing that of AuNPs electrodeposited on Gr or on MoS_2. This phenomenon can be attributed to the increased population of gold particles, a feature corroborated by observations in the SEM images. When scanning the potential in the opposite direction, a cathodic peak is recorded, which

corresponds to the electrochemical process of reducing the previously formed oxide back to its metallic form.

3.4. NO_2^- Oxidation on AuNPs Electrodeposited on Different Substrates

The electrocatalytic activity of the chemically modified electrodes—designated as AuNPs/Gr/SPE, AuNPs/MoS_2/SPE, and MoS_2-AuNPs/SPE—was investigated through cyclic voltammetry for nitrite oxidation. Figure 7 displays the voltammograms obtained for 0.2 mM $NaNO_2$ in 0.1 M H_2SO_4 using these three modified electrode configurations, compared to the nitrite response on a bare gold electrode (AuNPs/SPE) employed as a control. The anodic peak corresponding to the oxidation of nitrite to nitrate on electrodeposited AuNPs consistently appears at approximately the same potential (~0.5 ± 0.05 V) regardless of the type of 2D material used as the deposition substrate. The irreversible oxidation of nitrite is proposed to follow an electrochemical mechanism involving a two-electron transfer process, as described by Reaction (4).

$$NO_2^- + H_2 \rightarrow NO_3^- + 2H^+ + 2e^- \quad (4)$$

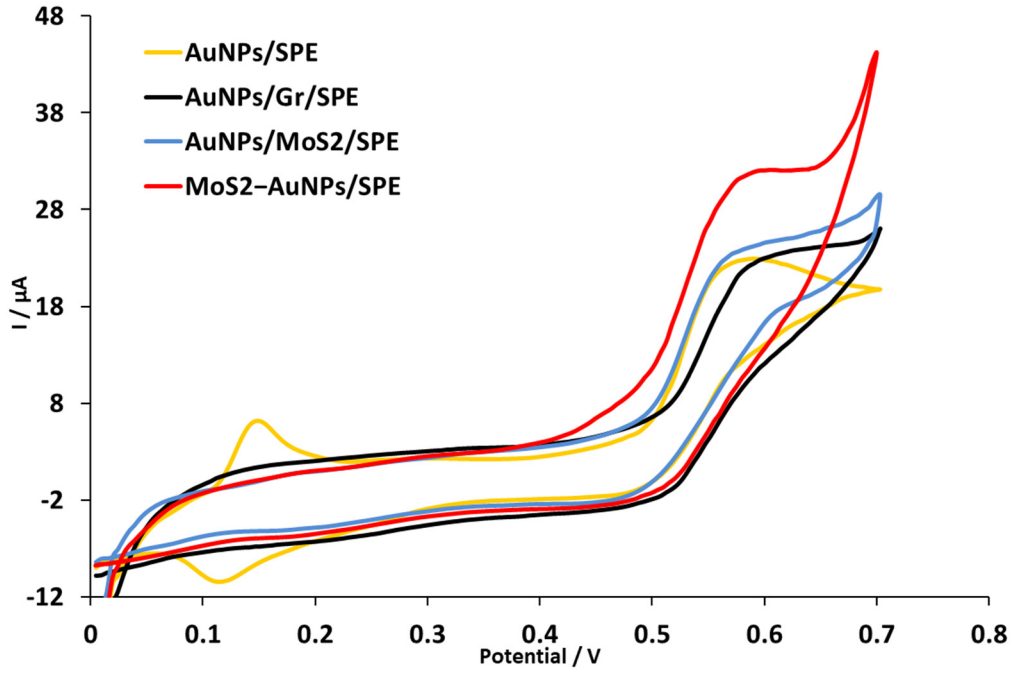

Figure 7. Voltammetric response for 0.2 mM $NaNO_2$ on chemically modified electrodes: AuNPs/SPE (yellow), AuNPs/Gr/SPE (black), AuNPs/MoS_2/SPE (blue) and MoS_2_AuNPs/SPE (red) in 0.1 M H_2SO_4.

The only difference noted lies in the heightened peak of nitrite oxidation on gold particles co-deposited with MoS_2 (MoS_2-AuNPs/SPE), significantly surpassing the nitrite oxidation peaks on AuNPs electrodeposited on the bare gold electrode or on 2D materials (Gr and MoS_2). This superior electrocatalytic performance of MoS_2-AuNPs/SPE toward nitrite can be attributed to the increased quantity of gold nanoparticles, as observed in both morphology and electrodeposition studies.

While the inclusion of 2D materials does not yield notable enhancements in the nitrite oxidation on AuNPs compared to SPE modified solely with nanoparticles, the chemically modified electrodes in this study exhibit a noteworthy advantage over other studies in the specialized literature concerning the oxidation potential of nitrite. In the present study, nitrite oxidation was obtained at a lower potential (0.5 V ± 0.05 V), compared to the

values of 0.8 V–1 V reported in other studies using AuNPs [66–69]. The electrocatalytic activity of gold nanoparticles co-deposited with MoS_2 is superior compared to that of AuNPs electrodeposited either on a bare electrode or on 2D materials (Gr and MoS_2). Hence, the (MoS_2-AuNPs/SPE) configuration appears to be a promising sensor for NO_2^- determination and will be further employed to refine the electrocatalytic detection of nitrite, paving the way for the development of an advanced electrochemical sensor.

3.5. Optimization of Co-Deposition of Gold Nanoparticles with MoS_2—Influence of Scanning Cycles

In the investigation of an electrocatalytic response to nitrite, the number and size of nanoparticles play a crucial role. To understand this influence, the impact of different deposition cycles was examined. Five electrodepositions were conducted by scanning the potential between +0.6 V and −1 V, each corresponding to a different number of cycles (1, 2, 3, 4, and 6 cycles). After electrodeposition, each electrode was examined by cyclic voltammetry with 0.4 mM nitrite in 0.1 M H_2SO_4 (Figure 8).

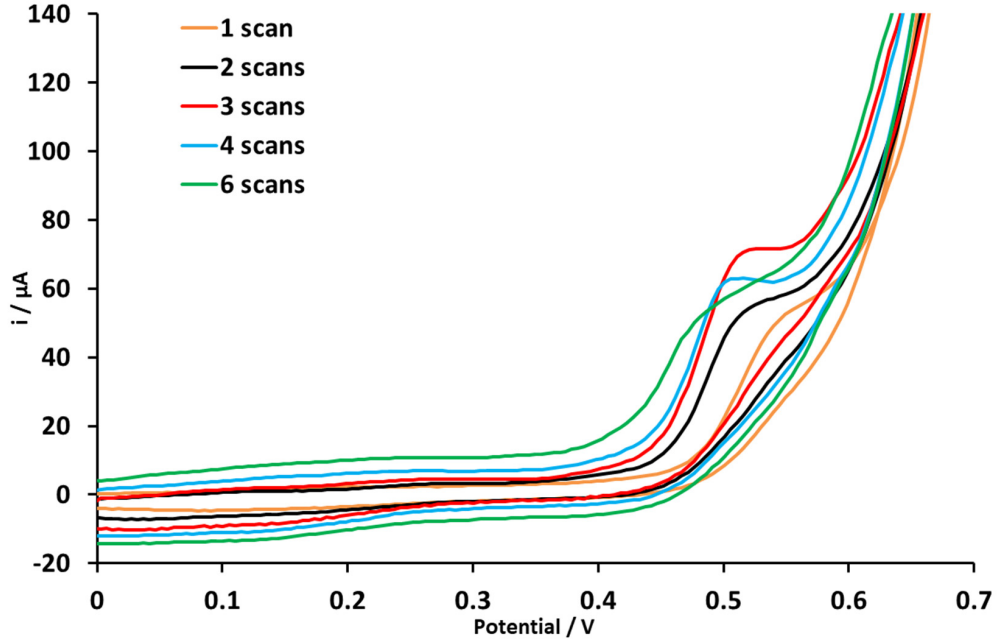

Figure 8. Voltammetric response for 0.4 mM $NaNO_2$ in 0.1 M H_2SO_4 on MoS_2_AuNPs/SPE prepared for different number of potential cycles: 1, 2, 3, 4, and 6.

The obtained results revealed a significant increase in the anodic peak current as the number of cycles increased, reaching a peak at nanoparticles deposited with three scans. This observation suggests that with an increasing number of deposition cycles, the rate of nucleation and growth also rises. However, beyond a certain threshold, excessive growth and aggregation of particles occur on the electrode surface. This phenomenon is reflected in the increase in the capacitive current of the MoS_2-AuNPs-electrode and subsequently, the decrease of the oxidation peak of nitrite, indicating the adverse effects of prolonged deposition cycles on the electrocatalytic behavior of the electrode.

3.6. Optimization of Co-Deposition of Gold Nanoparticles with MoS_2—Influence of MoS_2 Concentration

Since the addition of one component can change the deposition of the other, it is expected that the concentration of the two metals plays an important role in the formation of bimetallic nanomaterials and their catalytic performance as a consequence. Therefore, five electrodepositions were conducted using the same concentration of gold precursor

($HAuCl_4$ 10 mM) alongside varying concentrations of the MoS_2 solution: 0.25, 0.5, 1, 2, and 4 mg/mL. Their distinct responses to the oxidation of 0.2 mM $NaNO_2$ in 0.1 H_2SO_4 are presented in Figure 9. Notably, as the concentration of MoS_2 involved in the co-deposition increases, the anodic peak shows a consistent rise. However, at the highest concentration of 4 mg/mL, the peak becomes challenging to define and quantify accurately.

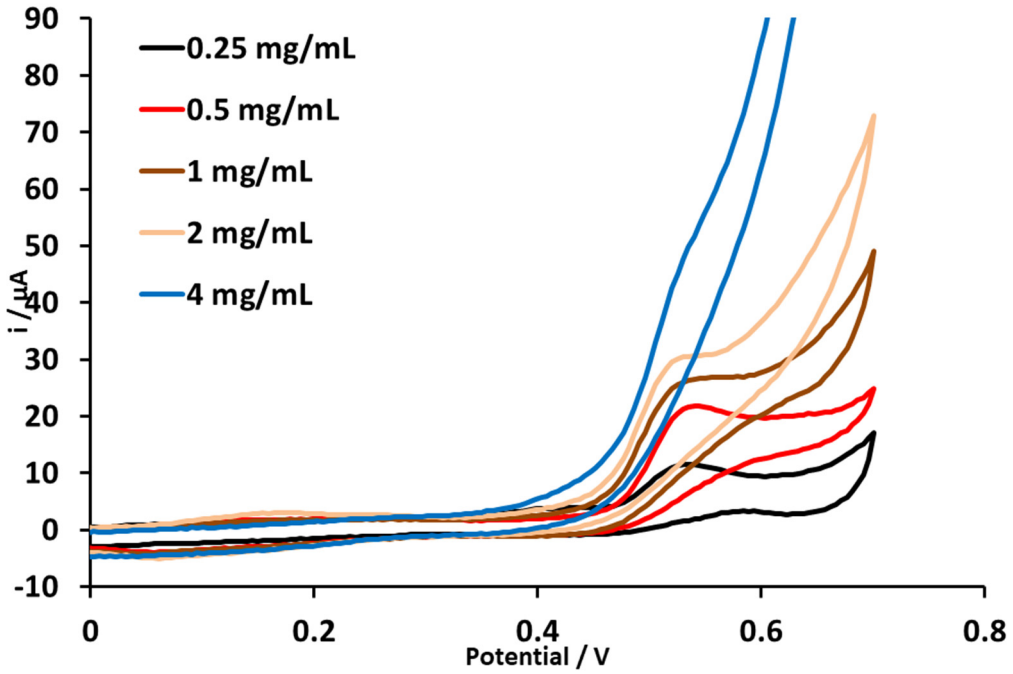

Figure 9. Voltametric response for 0.2 mM $NaNO_2$ in 0.1 H_2SO_4 on MoS_2_AuNPs/SPE prepared with different concentration of MoS_2: 0.25; 0.5; 1; 2 and 4 mg/mL.

To better understand the electrochemical mechanism of nitrite oxidation, the CV curves of 0.2 mM $NaNO_2$ in 0.1 H_2SO_4 were recorded at different scan rates from 10 and 200 mV/s for MoS_2-AuNPs/SPE prepared with 2 mg/mL MoS_2 (Figure 10a). The result showed that the anodic peak currents (I_{ox}) of MoS_2-AuNPs/SPE increased accordingly with the increase of the square root of the scan rate. Figure 10b indicates a good linear relationship of I_{ox} vs. $v^{1/2}$ from 10 and 200 mV/s (linear regression equations: $I_{ox} = 6.65 + 1.61v^{1/2}$, $R^2 = 0.9893$). These results reveal that the electrochemical oxidation of nitrite at MoS_2-AuNPs/SPE is a typical diffusion-controlled process.

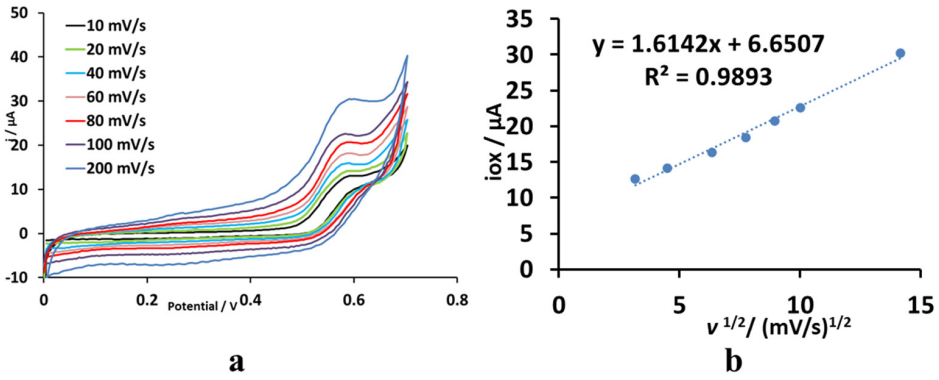

Figure 10. (**a**) CV curves of 0.2 mM $NaNO_2$ on MoS_2_AuNPs/SPE at different scan rates: 10, 20, 40, 60, 80, 100, and 200 mV/s. (**b**) Dependence of the oxidation peak current on the square root of scan rate.

3.7. Optimization of Nitrite Detection—Influence of the Applied Potential

The voltametric findings affirm the feasibility of nitrite oxidation using MoS_2-AuNPs/SPE, given appropriate optimization of working parameters for amperometric detection. Consequently, the influence of the applied potential was studied in order to enhance the sensor's performance for the utmost sensitivity in nitrite determination. To investigate this relationship, we examined four distinct values of the applied potential (0.5, 0.6, 0.7, and 0.8 V), measuring the resultant oxidation current as an indicator of the nitrite oxidation process.

According to the results depicted in Figure 11, the signal recorded for 0.1 mM nitrite increases proportionally with the applied potential until it reaches a threshold at 0.7 V. Beyond this point, at a higher potential (0.8 V), the recorded signal decreases. Consequently, the potential of 0.7 V will be adopted in subsequent experiments based on this observed trend.

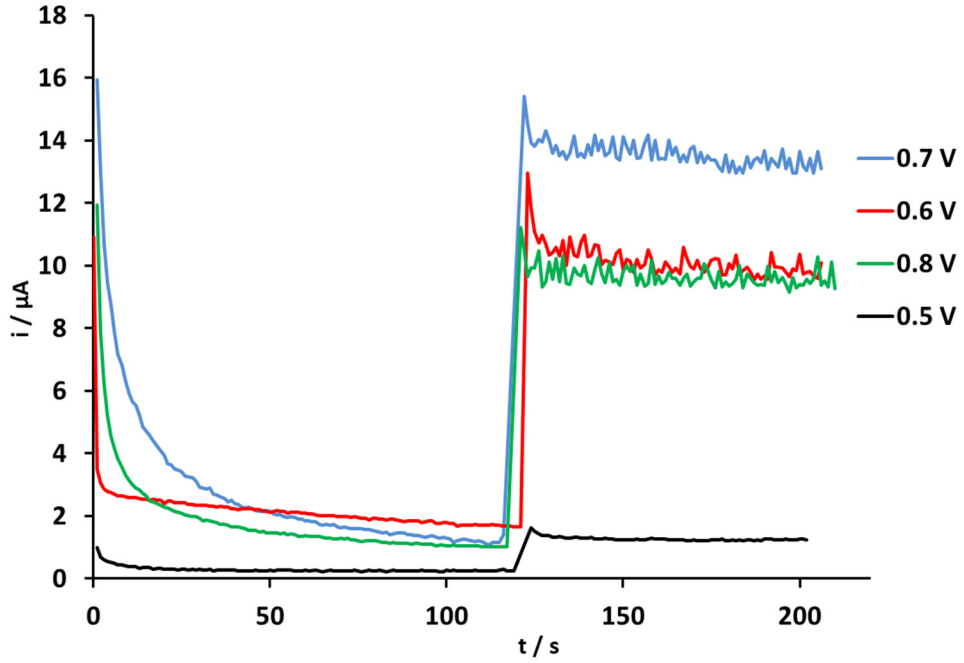

Figure 11. The amperometric response for 0.1 mM $NaNO_2$ in 0.1 M H_2SO_4 at different applied potentials: 0.5 V (black); 0.6 V (red); 0.7 V (blue) and 0.8 V (green).

3.8. Optimization of Nitrite Detection—Influence of Acid Concentration

Using the optimal applied potential of 0.7 V, the influence of H_2SO_4 concentration on the electrochemical oxidation reaction of nitrite was investigated using the MoS_2-AuNPs/SPE electrode. Figure 12 shows the amperometric response obtained for the oxidation of 0.1 mM nitrite, using different concentrations of the acid used as an electrolyte. The analytical signal demonstrates a positive correlation with the electrolyte concentration, peaking at 0.25 M. Subsequently, at a higher sulfuric acid concentration (0.5 M), the recorded current becomes less stable, exhibiting a decrease in intensity accompanied by an increase in noise. This phenomenon is attributed to the strongly acidic pH conditions, where the equilibrium of the reaction (reaction (4)) is not favored in the sense of oxidation, and the electronic transfer is correspondingly hindered. Consequently, for the following experiments, a sulfuric acid concentration of 0.25 M will be employed for all subsequent experiments in the electrochemical determination of nitrite, as it consistently delivered enhanced stability and a stronger oxidation current, thereby supporting improved sensitivity and overall sensor performance.

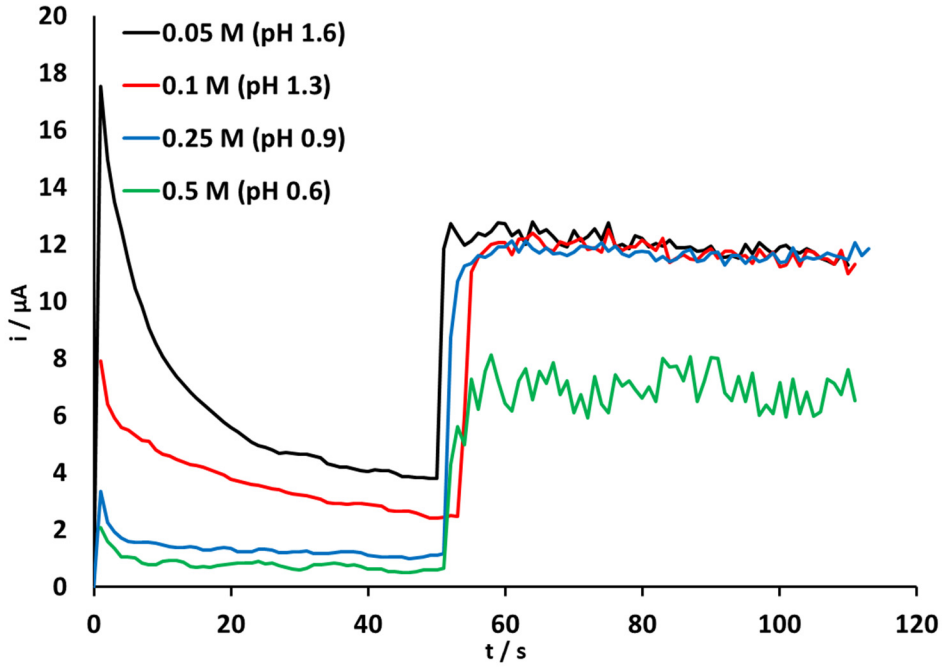

Figure 12. The amperometric response for 0.1 mM $NaNO_2$ in different concentrations of H_2SO_4: 0.05 M (black), 0.1 M (red), 0.25 M (blue) and 0.5 M (green); applied potential 0.7 V.

3.9. Calibration Curve

In order to evaluate the analytical performance of the chemically modified electrodes for the determination of nitrite, they were amperometrically calibrated by measuring the analytical signal for successive additions of nitrite in a 0.25 M H_2SO_4 electrolyte, applying a constant potential of 0.7 V, under continuous stirring. Figure 13a shows the nitrite oxidation current recorded over time for the MoS_2-AuNPs/SPE electrode (a) compared with the signal recorded for AuNPs/SPE (b) used as the control experiment. In both cases, for each addition of nitrite in the electrochemical cell, the oxidation current increased rapidly until it reached the maximum value and stabilized after 2–3 s. The increase of the recorded anodic current was directly proportional to the nitrite concentration in the linear ranges of 0.5–600 µM for the MoS_2-AuNPs/SPE configuration and 20–1300 µM for the AuNPs/SPE configuration.

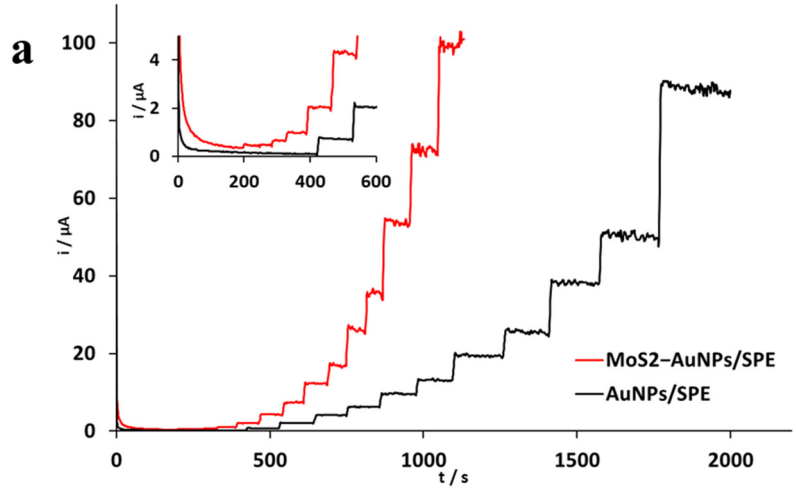

Figure 13. *Cont.*

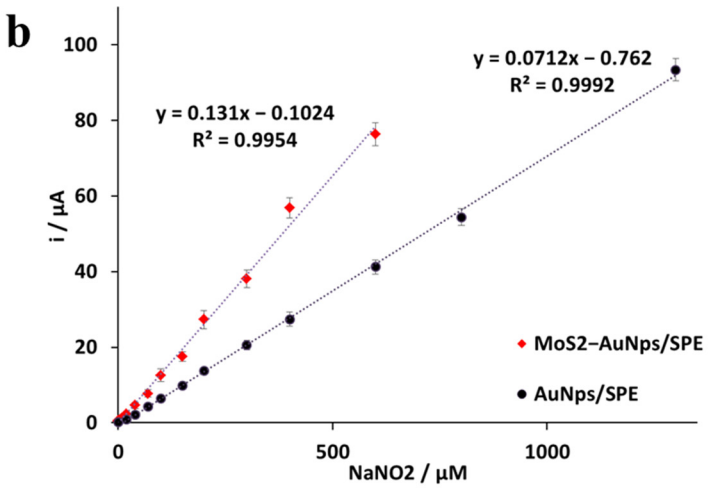

Figure 13. (**a**) Amperometric current response for successive additions of $NaNO_2$ in 0.25 M H_2SO_4, applied potential 0.7 V and (**b**) Calibration curve of $NaNO_2$ for modified electrodes: MoS_2-AuNPs/SPE and AuNPs/SPE; applied potential 0.7 V.

The oxidation currents recorded for the increasing concentrations were plotted as a function of the nitrite concentration, obtaining the calibration curves (Figure 13b). Analytical parameters, including sensor sensitivity (slope of the regression equation), the linear range of the response, and the limit of detection (for signal-to-noise ratio of 3) were estimated from these curves and are summarized in Table 2.

Table 2. Analytical parameters of AuNP modified electrodes for $NaNO_2$ detection developed in this work and compared to others from literature.

Modified Electrode	Detection Technique	Linear Range (µM)	Sensitivity (µA µM^{-1})	Specific Sensitivity (µA µM^{-1} cm^{-2})	Limit of Detection (µM)	Ref
AuNPs/SPE	Amperometry (0.7 V vs. Ag/AgCl)	20–1300	0.071	0.565	0.34	This work
MoS_2-AuNPs/SPE	Amperometry (0.7 V vs. Ag/AgCl)	0.5–600	0.131	1.043	0.16	This work
AuNPs/MoS_2/GN	Amperometry (0.75 V vs. SCE)	5–5000	0.0029	-	1	[66]
AuNPs/MXene/ERGO	Amperometry (0.83 V vs. Ag/AgCl)	0.5–80 80–780	0.024 0.069	0.34 0.977	0.15 0.015	[67]
Electrodeposited AuNp/SPCE	Square wave voltammetry (E_{ox} = 0.6 V vs. Ag)	1–300	0.453	-	0.38	[68]
AuNPs@MoS_2/rGO	Amperometry (0.804 V)	0.2–2600	0.158	0.805	0.038	[70]
AuNPs/MoS_2	Amperometry (0.8 V vs. Ag/AgCl)	5–27,800		117	1.67	[29]
Au-RGO/PDDA/GCE	DPV (E_{ox} = 0.85 V vs. SCE)	0.05–8.5	0.473	-	0.04	[71]
AuNP/MnOx-VOx/ERGO	Amperometry (0.8 V vs. Ag/AgCl)	1–100	0.05	-	0.1	[42]

The oxidation of nitrite on MoS_2-AuNPs/SPE benefits from the greater quantity of gold nanoparticles formed during the co-deposition with MoS_2. As previously discussed, the co-deposition process results in a significantly larger contact surface, facilitating the deposition of a greater number of gold nanoparticles.

These results emphasize the ability of MoS_2-AuNPs/SPE electrodes to detect nitrite at very low concentrations, thus providing sensitivity and precision in the electrochemical analysis of this compound. The results obtained are comparable or superior to other data reported in the literature for electrochemical sensors based on gold nanoparticles used in the determination of nitrite [30,67,69].

3.10. Interferences Study

To evaluate the selectivity of the MoS_2-AuNPs/SPE electrode to nitrite, several substances that commonly coexist with NO_2^- in real samples were tested. These included KCl, $MgCO_3$, $CaCl_2$, $NaNO_3$, $MgSO_4$, glucose, and NaCl, which might undergo oxidation at

the potential applied for nitrite detection, potentially interfering with its determination using the amperometric method. The compounds were tested under previously optimized conditions (applied potential of 0.7 V and H_2SO_4 0.25 M), with each taken in excess compared to the nitrite concentration. High concentration of these substances was strategically chosen to represent a realistic range of concentrations that could be encountered in diverse real-world scenarios (biological or environmental samples).

In contrast to the noticeable increase in current upon the addition of $NaNO_2$, the alterations induced by the introduction of these interferents are negligible (Figure 14). This suggests a highly selective detection of $NaNO_2$ using the optimized MoS_2-AuNPs/SPE electrodes.

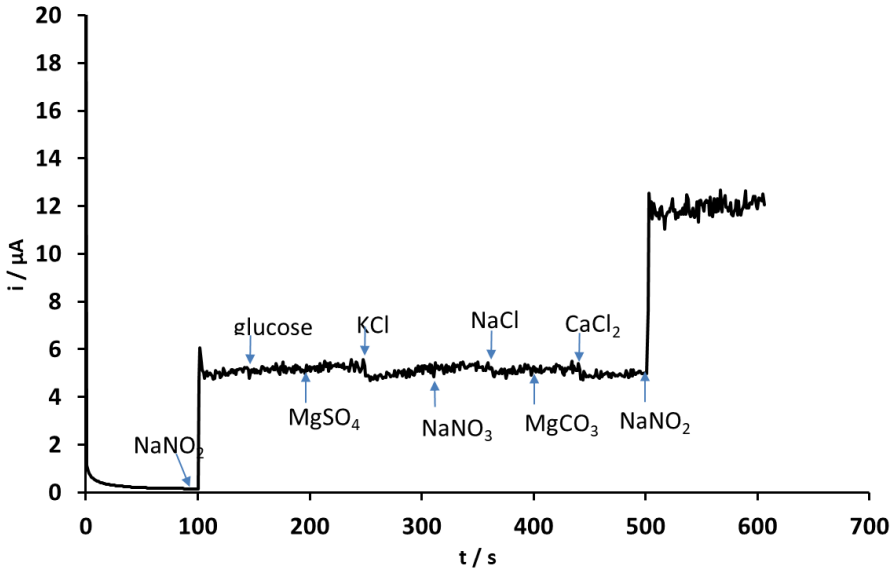

Figure 14. The amperometric response of MoS_2-AuNPs/SPE electrode to the successive addition of: 10 µM $NaNO_2$ and 50 µM glucose, $MgSO_4$, KCl, $NaNO_3$, NaCl, $MgCO_3$, and $CaCl_2$.

4. Conclusions

This study conducts a comparative analysis of the electrocatalytic activity of gold nanoparticles electrodeposited on various two-dimensional materials (Gr and MoS_2). Two distinct approaches were employed: (i) electrodeposition of AuNPs on Gr and MoS_2, and (ii) co-deposition with MoS_2. The electrodeposition process of gold nanoparticles was performed by cyclic voltammetry, revealing the insignificant influence of the substrate material when nanoparticles are anchored on the 2D materials, but that some differences appear when gold nanoparticles are co-deposited with MoS_2.

All of the AuNPs obtained through electrodeposition on Gr and MoS_2 or co-deposited with MoS_2 underwent morphological and electrochemical characterization. The results demonstrated the efficacy of the co-deposition process with MoS_2, highlighting the preference of gold for specific attachment sites on MoS_2, particularly at edges and defects. Their electrocatalytic activity was evaluated against nitrite oxidation, confirming the efficiency of the co-deposition of gold nanoparticles with MoS_2. The developed electrochemical sensor, MoS_2-AuNPs/SPE, exhibits high sensitivity for nitrite detection, with an oxidation peak occurring at a low potential of approximately 0.5 V. It is capable of detecting low concentrations of nitrite, achieving a limit of detection (LOD) of 0.16 µM, and demonstrates excellent selectivity as it is not affected by the presence of other common biological compounds. Beyond its electrochemical performance, the sensor also offers practical advantages, including rapid response and ease of fabrication, making it a strong candidate for real-world applications such as environmental monitoring of water quality and food safety analysis,

where reliable detection of nitrite under varying sample conditions is critical. Its simple and scalable design makes it suitable for integration into portable devices. Future studies will focus on optimizing its performance and evaluating its stability under different pH conditions, aiming to further enhance its practical applicability.

Author Contributions: A.A. and O.E.C. was responsible for conceptualization, methodology, validation, writing—original draft and preparation, A.A. and M.P. for formal analysis, writing—review and editing, supervision and project administration, O.E.C. and M.-F.Z. for investigation and data curation, M.P. for funding and acquisition. All authors have read and agreed to the published version of the manuscript.

Funding: This research was funded by project no. PNRR-III-C9-2023-I8-161, contract no. 760285/27.03.2024, within the National Recovery and Resilience Plan.

Institutional Review Board Statement: Not applicable.

Informed Consent Statement: Not applicable.

Data Availability Statement: The raw data supporting the conclusions of this article will be made available by the authors on request.

Acknowledgments: The authors thank the financial support of the grant of the Ministry of Research, Innovation and Digitization, project no. PNRR-III-C9-2023-I8-161, contract no. 760285/27.03.2024, within the National Recovery and Resilience Plan.

Conflicts of Interest: The authors declare that they have no competing interests.

Abbreviations

The following abbreviations are used in this manuscript:

Gr	Graphene
2DMs	Two-dimensional materials
NPs	Nanoparticles
AuNPs	Gold nanoparticles
SEM	Scanning electron microscopy
FTIR	Fourier transform infrared (FTIR)
CV	Cyclic voltammetry
SPE	Screen-printed electrode

References

1. Xiong, Z.; Zhong, L.; Wang, H.; Li, X. Structural defects, mechanical behaviors, and properties of two-dimensional materials. *Materials* **2021**, *14*, 1192. [CrossRef] [PubMed]
2. Kanungo, S.; Ahmad, G.; Sahatiya, P.; Mukhopadhyay, A.; Chattopadhyay, S. 2D materials-based nanoscale tunneling field effect transistors: Current developments and future prospects. *npj 2D Mater. Appl.* **2022**, *6*, 83. [CrossRef]
3. Wang, H.; Yuan, H.; Hong, S.S.; Li, Y.; Cui, Y. Physical and chemical tuning of two-dimensional transition metal dichalcogenides. *Chem. Soc. Rev.* **2015**, *44*, 2664–2680. [CrossRef] [PubMed]
4. Duan, X.; Wang, C.; Pan, A.; Yu, R.; Duan, X. Two-dimensional transition metal dichalcogenides as atomically thin semiconductors: Opportunities and challenges. *Chem. Soc. Rev.* **2015**, *44*, 8859–8876. [CrossRef]
5. Özdokur, K.V.; Tatlı, A.Y.; Yılmaz, B.; Koçak, S.; Ertaş, F.N. Development of pulsed deposited manganese and molybdenum oxide surfaces decorated with platinum nanoparticles and their catalytic application for formaldehyde oxidation. *Int. J. Hydrogen Energy* **2016**, *41*, 5927–5933. [CrossRef]
6. Sun, T.; Zhang, G.; Xu, D.; Lian, X.; Li, H.; Chen, W.; Su, C. Defect chemistry in 2D materials for electrocatalysis. *Mater. Today Energy* **2019**, *12*, 215–238. [CrossRef]
7. Mohammadniaei, M.; Nguyen, H.V.; Tieu, M.V.; Lee, M.-H. 2D materials in development of electrochemical point-of-care cancer screening devices. *Micromachines* **2019**, *10*, 662. [CrossRef]
8. Hajian, R.; Fung, K.; Chou, P.P.; Wang, S.; Balderston, S.; Aran, K. Properties and applications of functionalized graphene oxide. *Mater. Matters* **2019**, *14*, 1–15.

9. Weiss, N.O.; Zhou, H.; Liao, L.; Liu, Y.; Jiang, S.; Huang, Y.; Duan, X. Graphene: An emerging electronic material. *Adv. Mater.* **2012**, *24*, 5782–5825. [CrossRef]
10. Huang, H.; Su, S.; Wu, N.; Wan, H.; Wan, S.; Bi, H.; Sun, L. Graphene-based sensors for human health monitoring. *Front. Chem.* **2019**, *7*, 399. [CrossRef]
11. Zeng, M.; Xiao, Y.; Liu, J.; Yang, K.; Fu, L. Exploring two-dimensional materials toward the next-generation circuits: From monomer design to assembly control. *Chem. Rev.* **2018**, *118*, 6236–6296. [CrossRef] [PubMed]
12. Zhu, J.; Ha, E.; Zhao, G.; Zhou, Y.; Huang, D.; Yue, G.; Hu, L.; Sun, N.; Wang, Y.; Lee, L.Y.S. Recent advance in MXenes: A promising 2D material for catalysis, sensor and chemical adsorption. *Coord. Chem. Rev.* **2017**, *352*, 306–327. [CrossRef]
13. Zou, H.L.; Li, B.L.; Luo, H.Q.; Li, N.B. 0D-2D heterostructures of Au nanoparticles and layered MoS_2 for simultaneous detections of dopamine, ascorbic acid, uric acid, and nitrite. *Sens. Actuators B Chem.* **2017**, *253*, 352–360. [CrossRef]
14. Van Tuan, D.; Ngan, D.T.T.; Thuy, N.T.; Lan, H.; Nguyet, N.T.; Van Thu, V.; Hung, V.-P.; Tam, P.D. Effect of nanostructured MoS_2 morphology on the glucose sensing of electrochemical biosensors. *Curr. Appl. Phys.* **2020**, *20*, 1090–1096. [CrossRef]
15. Koçak, S.; Ertaş, F.N.; Dursun, Z. Electrochemical deposition and behavior of mixed-valent molybdenum oxide film at glassy carbon and ITO electrodes. *Appl. Surf. Sci.* **2013**, *265*, 205–213. [CrossRef]
16. Mbayachi, V.B.; Ndayiragije, E.; Sammani, T.; Taj, S.; Mbuta, E.R. Graphene synthesis, characterization and its applications: A review. *Results Chem.* **2021**, *3*, 100163. [CrossRef]
17. Zhang, T.; Gao, X.; Li, J.; Xiao, L.; Gao, H.; Zhao, F.; Ma, H. Progress on the application of graphene-based composites toward energetic materials: A review. *Def. Technol.* **2024**, *31*, 95–116. [CrossRef]
18. Kamboj, S.; Thakur, A. Applications of Graphene-Based Composites-A Review. *Mater. Today Proc.* **2023**, in press. [CrossRef]
19. Fu, Y.; Yang, Y.; Tuersun, T.; Yu, Y.; Zhi, J. Simple preparation and highly selective detection of silver ions using an electrochemical sensor based on sulfur-doped graphene and a 3, 3′, 5, 5′-tetramethylbenzidine composite modified electrode. *Analyst* **2018**, *143*, 2076–2082. [CrossRef]
20. Krishnan, U.; Kaur, M.; Singh, K.; Kumar, M.; Kumar, A. A synoptic review of MoS_2: Synthesis to applications. *Superlattices Microstruct.* **2019**, *128*, 274–297. [CrossRef]
21. Du, C.; Shang, A.; Shang, M.; Zhang, J.; Song, W. Surface-functionalized MoS_2 ultrathin nanosheets for electrochemical monitoring terminal deoxynucleotidyl transferase activity based on in-situ polymerized DNA. *Sens. Actuators B Chem.* **2018**, *277*, 297–305. [CrossRef]
22. Zhai, Y.; Li, J.; Chu, X.; Xu, M.; Jin, F.; Li, X.; Fang, X.; Wei, Z.; Wang, X. MoS_2 microflowers based electrochemical sensing platform for non-enzymatic glucose detection. *J. Alloys Compd.* **2016**, *672*, 600–608. [CrossRef]
23. Wang, T.; Du, K.; Liu, W.; Zhang, J.; Li, M. Electrochemical sensors based on molybdenum disulfide nanomaterials. *Electroanalysis* **2015**, *27*, 2091–2097. [CrossRef]
24. Li, T.; Shang, D.; Gao, S.; Wang, B.; Kong, H.; Yang, G.; Shu, W.; Xu, P.; Wei, G. Two-dimensional material-based electrochemical sensors/biosensors for food safety and biomolecular detection. *Biosensors* **2022**, *12*, 314. [CrossRef]
25. Liu, H.; Jiang, H.; Liu, X.; Wang, X. *Physicochemical Understanding of Biomineralization by Molecular Vibrational Spectroscopy: From Mechanism to Nature, Exploration, 2023*; Wiley Online Library: Hoboken, NJ, USA, 2023; p. 20230033.
26. Huang, K.-J.; Zhang, J.-Z.; Liu, Y.-J.; Wang, L.-L. Novel electrochemical sensing platform based on molybdenum disulfide nanosheets-polyaniline composites and Au nanoparticles. *Sens. Actuators B Chem.* **2014**, *194*, 303–310. [CrossRef]
27. Gan, X.; Zhao, H.; Quan, X. Two-dimensional MoS_2: A promising building block for biosensors. *Biosens. Bioelectron.* **2017**, *89*, 56–71. [CrossRef]
28. Yang, Y.; Zhang, H.; Huang, C.; Yang, D.; Jia, N. Electrochemical non-enzyme sensor for detecting clenbuterol (CLB) based on MoS2-Au-PEI-hemin layered nanocomposites. *Biosens. Bioelectron.* **2017**, *89*, 461–467. [CrossRef]
29. Zhang, S.; Tang, Y.; Chen, Y.; Zheng, J. Synthesis of gold nanoparticles coated on flower-like MoS_2 microsphere and their application for electrochemical nitrite sensing. *J. Electroanal. Chem.* **2019**, *839*, 195–201. [CrossRef]
30. Zhang, X.; Sun, R. Construction of an electrochemical sensor for detection of nitrite by gold nanoparticles immobilized on biochar. *Int. J. Electrochem. Sci.* **2023**, *18*, 100219. [CrossRef]
31. Siciliano, G.; Alsadig, A.; Chiriacò, M.S.; Turco, A.; Foscarini, A.; Ferrara, F.; Gigli, G.; Primiceri, E. Beyond traditional biosensors: Recent advances in gold nanoparticles modified electrodes for biosensing applications. *Talanta* **2024**, *268*, 125280. [CrossRef]
32. Thanh, T.D.; Balamurugan, J.; Hwang, J.Y.; Kim, N.H.; Lee, J.H. In situ synthesis of graphene-encapsulated gold nanoparticle hybrid electrodes for non-enzymatic glucose sensing. *Carbon* **2016**, *98*, 90–98. [CrossRef]
33. Ju, J.; Chen, W. In situ growth of surfactant-free gold nanoparticles on nitrogen-doped graphene quantum dots for electrochemical detection of hydrogen peroxide in biological environments. *Anal. Chem.* **2015**, *87*, 1903–1910. [CrossRef] [PubMed]
34. Liu, C.; Wang, K.; Luo, S.; Tang, Y.; Chen, L. Direct electrodeposition of graphene enabling the one-step synthesis of graphene–metal nanocomposite films. *Small* **2011**, *7*, 1203–1206. [CrossRef] [PubMed]
35. Chen, N.; Cheng, Y.; Li, C.; Zhang, C.; Zhao, K.; Xian, Y. Determination of melamine in food contact materials using an electrode modified with gold nanoparticles and reduced graphene oxide. *Microchim. Acta* **2015**, *182*, 1967–1975. [CrossRef]

36. Ding, L.; Liu, Y.; Zhai, J.; Bond, A.M.; Zhang, J. Direct electrodeposition of graphene-gold nanocomposite films for ultrasensitive voltammetric determination of mercury (II). *Electroanalysis* **2014**, *26*, 121–128. [CrossRef]
37. Xu, Y.; Zhang, W.; Shi, J.; Zou, X.; Li, Y.; Elrasheid, T.H.; Huang, X.; Li, Z.; Zhai, X.; Hu, X. Electrodeposition of gold nanoparticles and reduced graphene oxide on an electrode for fast and sensitive determination of methylmercury in fish. *Food Chem.* **2017**, *237*, 423–430. [CrossRef]
38. Jian, J.-M.; Fu, L.; Ji, J.; Lin, L.; Guo, X.; Ren, T.-L. Electrochemically reduced graphene oxide/gold nanoparticles composite modified screen-printed carbon electrode for effective electrocatalytic analysis of nitrite in foods. *Sens. Actuators B Chem.* **2018**, *262*, 125–136. [CrossRef]
39. Li, S.-J.; Zhao, G.-Y.; Zhang, R.-X.; Hou, Y.-L.; Liu, L.; Pang, H. A sensitive and selective nitrite sensor based on a glassy carbon electrode modified with gold nanoparticles and sulfonated graphene. *Microchim. Acta* **2013**, *180*, 821–827. [CrossRef]
40. He, B.-S.; Yan, D.-D. One-pot preparation of wavy graphene/Au composites and their application for highly sensitive detection of nitrite. *Anal. Methods* **2018**, *10*, 3654–3659. [CrossRef]
41. Ye, D.; Luo, L.; Ding, Y.; Chen, Q.; Liu, X. A novel nitrite sensor based on graphene/polypyrrole/chitosan nanocomposite modified glassy carbon electrode. *Analyst* **2011**, *136*, 4563–4569. [CrossRef]
42. Aslışen, B.; Koçak, S. Preparation of mixed-valent manganese-vanadium oxide and Au nanoparticle modified graphene oxide nanosheets electrodes for the simultaneous determination of hydrazine and nitrite. *J. Electroanal. Chem.* **2022**, *904*, 115875. [CrossRef]
43. Zhu, X.; He, M.; Xiao, L.; Liu, H.; Hu, M.; Li, S.; Zhai, Q.-G.; Chen, Y.; Jiang, Y. Enzymatic biosensor for nitrite detection based on direct electron transfer by CPO-ILEMB/Au@MoS_2/GC. *J. Appl. Electrochem.* **2022**, *52*, 979–987. [CrossRef]
44. Li, X.; Zou, N.; Wang, Z.; Sun, Y.; Li, H.; Gao, C.; Wang, T.; Wang, X. An electrochemical sensor for determination of nitrite based on Au nanoparticles decorated MoS_2 nanosheets. *Chem. Pap.* **2020**, *74*, 441–449. [CrossRef]
45. Afkhami, A.; Soltani-Felehgari, F.; Madrakian, T.; Ghaedi, H. Surface decoration of multi-walled carbon nanotubes modified carbon paste electrode with gold nanoparticles for electro-oxidation and sensitive determination of nitrite. *Biosens. Bioelectron.* **2014**, *51*, 379–385. [CrossRef]
46. Zhuang, Z.; Lin, H.; Zhang, X.; Qiu, F.; Yang, H. A glassy carbon electrode modified with carbon dots and gold nanoparticles for enhanced electrocatalytic oxidation and detection of nitrite. *Microchim. Acta* **2016**, *183*, 2807–2814. [CrossRef]
47. Rajkumar, C.; Thirumalraj, B.; Chen, S.-M.; Palanisamy, S. Novel electrochemical preparation of gold nanoparticles decorated on a reduced graphene oxide–fullerene composite for the highly sensitive electrochemical detection of nitrite. *RSC Adv.* **2016**, *6*, 68798–68805. [CrossRef]
48. Zou, C.; Yang, B.; Bin, D.; Wang, J.; Li, S.; Yang, P.; Wang, C.; Shiraishi, Y.; Du, Y. Electrochemical synthesis of gold nanoparticles decorated flower-like graphene for high sensitivity detection of nitrite. *J. Colloid Interface Sci.* **2017**, *488*, 135–141. [CrossRef]
49. Hatip, M.; Koçak, S.; Dursun, Z. Simultaneous electrochemical determination of hydrazine and nitrite based on Au nanoparticles decorated on the poly (Nile Blue) modified carbon nanotube. *Electroanalysis* **2023**, *35*, e202200132. [CrossRef]
50. Shanmugam, M.; Kim, K. Electrodeposited gold dendrites at reduced graphene oxide as an electrocatalyst for nitrite and glucose oxidation. *J. Electroanal. Chem.* **2016**, *776*, 82–92. [CrossRef]
51. Arvinte, A.; Crudu, I.-A.; Doroftei, F.; Timpu, D.; Pinteala, M. Electrochemical codeposition of silver-gold nanoparticles on CNT-based electrode and their performance in electrocatalysis of dopamine. *J. Electroanal. Chem.* **2018**, *829*, 184–193. [CrossRef]
52. Chiang, H.-C.; Wang, Y.; Zhang, Q.; Levon, K. Optimization of the Electrodeposition of Gold Nanoparticles for the Application of Highly Sensitive, Label-Free Biosensor. *Biosensors* **2019**, *9*, 50. [CrossRef] [PubMed]
53. Hezard, T.; Fajerwerg, K.; Evrard, D.; Collière, V.; Behra, P.; Gros, P. Gold nanoparticles electrodeposited on glassy carbon using cyclic voltammetry: Application to Hg(II) trace analysis. *J. Electroanal. Chem.* **2012**, *664*, 46–52. [CrossRef]
54. O'Mullane, A.P.; Ippolito, S.J.; Sabri, Y.M.; Bansal, V.; Bhargava, S.K. Premonolayer Oxidation of Nanostructured Gold: An Important Factor Influencing Electrocatalytic Activity. *Langmuir* **2009**, *25*, 3845–3852. [CrossRef] [PubMed]
55. Huang, S.; Ma, H.; Zhang, X.; Yong, F.; Feng, X.; Pan, W.; Wang, X.; Wang, Y.; Chen, S. Electrochemical synthesis of gold nanocrystals and their 1D and 2D organization. *J. Phys. Chem. B* **2005**, *109*, 19823–19830. [CrossRef] [PubMed]
56. Sreeprasad, T.S.; Nguyen, P.; Kim, N.; Berry, V. Controlled, Defect-Guided, Metal-Nanoparticle Incorporation onto MoS_2 via Chemical and Microwave Routes: Electrical, Thermal, and Structural Properties. *Nano Lett.* **2013**, *13*, 4434–4441. [CrossRef]
57. Zhou, J.; Zhao, Y.; Bao, J.; Huo, D.; Fa, H.; Shen, X.; Hou, C. One-step electrodeposition of Au-Pt bimetallic nanoparticles on MoS_2 nanoflowers for hydrogen peroxide enzyme-free electrochemical sensor. *Electrochim. Acta* **2017**, *250*, 152–158. [CrossRef]
58. Daniel, M.-C.; Astruc, D. Gold nanoparticles: Assembly, supramolecular chemistry, quantum-size-related properties, and applications toward biology, catalysis, and nanotechnology. *Chem. Rev.* **2004**, *104*, 293–346. [CrossRef]
59. Landolt, D. Electrochemical and materials science aspects of alloy deposition. *Electrochim. Acta* **1994**, *39*, 1075–1090. [CrossRef]
60. Podlaha, E.J.; Landolt, D. Induced Codeposition: III. Molybdenum Alloys with Nickel, Cobalt, and Iron. *J. Electrochem. Soc.* **1997**, *144*, 1672. [CrossRef]

61. Wang, Y.; Laborda, E.; Crossley, A.; Compton, R.G. Surface oxidation of gold nanoparticles supported on a glassy carbon electrode in sulphuric acid medium: Contrasts with the behaviour of 'macro' gold. *Phys. Chem. Chem. Phys.* **2013**, *15*, 3133–3136. [CrossRef]
62. Xiang, C.; Güell, A.G.; Brown, M.A.; Kim, J.Y.; Hemminger, J.C.; Penner, R.M. Coupled electrooxidation and electrical conduction in a single gold nanowire. *Nano Lett.* **2008**, *8*, 3017–3022. [CrossRef]
63. Angerstein-Kozlowska, H.; Conway, B.E.; Hamelin, A.; Stoicoviciu, L. Elementary steps of electrochemical oxidation of single-crystal planes of Au Part II. A chemical and structural basis of oxidation of the (111) plane. *J. Electroanal. Chem. Interfacial Electrochem.* **1987**, *228*, 429–453. [CrossRef]
64. Angerstein-Kozlowska, H.; Conway, B.E.; Hamelin, A.; Stoicoviciu, L. Elementary steps of electrochemical oxidation of single-crystal planes of Au—I. Chemical basis of processes involving geometry of anions and the electrode surfaces. *Electrochim. Acta* **1986**, *31*, 1051–1061. [CrossRef]
65. Saldan, I.; Dobrovetska, O.; Sus, L.; Makota, O.; Pereviznyk, O.; Kuntyi, O.; Reshetnyak, O. Electrochemical synthesis and properties of gold nanomaterials. *J. Solid State Electrochem.* **2018**, *22*, 637–656. [CrossRef]
66. Han, Y.; Zhang, R.; Dong, C.; Cheng, F.; Guo, Y. Sensitive electrochemical sensor for nitrite ions based on rose-like AuNPs/MoS_2/graphene composite. *Biosens. Bioelectron.* **2019**, *142*, 111529. [CrossRef]
67. Wang, T.; Wang, C.; Xu, X.; Li, Z.; Li, D. One-Step Electrodeposition Synthesized Aunps/Mxene/ERGO for Selectivity Nitrite Sensing. *Nanomaterials* **2021**, *11*, 1892. [CrossRef]
68. Adiraju, A.; Munjal, R.; Viehweger, C.; Al-Hamry, A.; Brahem, A.; Hussain, J.; Kommisetty, S.; Jalasutram, A.; Tegenkamp, C.; Kanoun, O. Towards Embedded Electrochemical Sensors for On-Site Nitrite Detection by Gold Nanoparticles Modified Screen Printed Carbon Electrodes. *Sensors* **2023**, *23*, 2961. [CrossRef]
69. Wang, Y.; Zeng, Z.; Qiao, J.; Dong, S.; Liang, Q.; Shao, S. Ultrasensitive determination of nitrite based on electrochemical platform of AuNPs deposited on PDDA-modified MXene nanosheets. *Talanta* **2021**, *221*, 121605. [CrossRef]
70. Yang, Y.; Lei, Q.; Li, J.; Hong, C.; Zhao, Z.; Xu, H.; Hu, J. Synthesis and enhanced electrochemical properties of AuNPs@ MoS_2/rGO hybrid structures for highly sensitive nitrite detection. *Microchem. J.* **2022**, *172*, 106904. [CrossRef]
71. Jiao, S.; Jin, J.; Wang, L. One-pot preparation of Au-RGO/PDDA nanocomposites and their application for nitrite sensing. *Sens. Actuators B Chem.* **2015**, *208*, 36–42. [CrossRef]

Disclaimer/Publisher's Note: The statements, opinions and data contained in all publications are solely those of the individual author(s) and contributor(s) and not of MDPI and/or the editor(s). MDPI and/or the editor(s) disclaim responsibility for any injury to people or property resulting from any ideas, methods, instructions or products referred to in the content.